

# Robust Correction of Interferometer Phase Drift in Transmission Matrix Measurements

RALF MOUTHAAAN<sup>1,2</sup>, PETER CHRISTOPHER<sup>2</sup>, GEORGE GORDON<sup>3</sup>,  
TIMOTHY WILKINSON<sup>2</sup> AND TIJMEN G. EUSER<sup>1,\*</sup>

<sup>1</sup> *Nanophotonics Centre, Cavendish Laboratory (University of Cambridge, UK)*

<sup>2</sup> *CMMPE, Electrical Engineering Department (University of Cambridge, UK)*

<sup>3</sup> *Electrical Engineering Department (University of Nottingham, UK)*

\*[te287@cam.ac.uk](mailto:te287@cam.ac.uk)

**Abstract:** A complex-valued transmission matrix describing a scattering medium can be constructed from a sequence of many interferometric measurements. A major challenge in such experiments is to correct for rapid phase drift of the optical system during the data acquisition process, especially when the phase drifts significantly between consecutive measurements. Therefore, a new method is presented whereby the exact phase drift between two measurements is characterised and corrected for using a single additional measurement. This approach removes the need to continuously track the phase and significantly relaxes the phase stability requirements of the interferometer, allowing transmission matrices to be constructed in the presence of fast and erratic phase drift.

© 2022 Optical Society of America

## 1. Introduction

The interaction of light with a scattering medium such as white paint [1–4] or biological tissue [5–7] severely distorts the incident wavefront. Similarly, light is distorted when travelling through a multimode waveguide [8–10]. Wavefront shaping techniques allow this distortion to be characterized and corrected for, permitting images to be acquired from the far side of these scattering media. Recent advances in wavefront shaping are now enabling new imaging techniques, such as hair-thin endoscopes [9, 11, 12] and microscopes capable of imaging at depths beyond the scattering mean free path [3, 7, 13].

The distortion imposed by a scattering medium is linear, and can therefore be described by a transmission matrix [14, 15]. The transmission matrix is usually constructed by coupling a sequence of input fields through the scattering medium and observing the resultant output fields. As the transmission matrix is complex-valued, the output field is typically measured using an interferometer.

In interferometry, the relative phase offset between the object beam and the reference beam can drift in time due to airflow, wavelength drift, temperature variations and mechanical vibrations. Several approaches have been taken in different experimental contexts to correct for this phase drift. For example, multiple reference channels can be used to isolate and correct the phase drift in an optical sensor based on a Young’s interferometer [16]. In Mach-Zehnder-based refractometers, a secondary reference beam that travels the same path as the object beam can be used to correct drift [17]. Phase drift in a holographic recording system was monitored using homodyne detection techniques and corrected by a piezo-controlled mirror [18]. Roztocki et al. use two signals in quadrature to detect any phase shifts and dynamically correct for these using a fiber stretcher [19]. Finally, it is also possible to mechanically isolate the system from its environment to minimize any phase drift. This approach is taken in the Laser Interferometer Gravitational-Wave Observatory (LIGO) [20].

Many thousands of interferometer measurements are typically required when constructing a transmission matrix. Therefore, the relative phase offset between the interferometer reference

beam and the interferometer object beam must be kept stable over an extended period. Alternatively, periodic reference measurements can be used to correct the phase drift at intermediary intervals. These requirements can become onerous in the presence of rapid phase drift. To overcome this limitation, we present a new off-axis holography approach that guarantees that any phase drift between the two interferometer arms is compensated for. Uniquely, even very rapid and erratic phase drift can be corrected using the proposed technique.

## 2. Background

Considering only the forward propagation direction, light propagation in a scattering medium can be described by a transmission matrix  $\mathbf{T}$  that relates the input fields  $E_{in}$  to the output fields  $E_{out}$ ,

$$E_{out} = \mathbf{T}E_{in}. \quad (1)$$

To construct the transmission matrix, a sequence of input fields is projected onto the scattering sample, and the resulting output fields are measured using an interferometer. Experimentally, this involves mixing the object beam, which has travelled through the scattering medium, with a reference beam. An interference pattern is formed, the intensity of which is captured using a camera. Two approaches are commonly taken to determine the complex-valued field of the object beam, namely *phase stepping holography* and *off-axis holography*.

### 2.1. Phase Stepping Holography

In phase stepping holography [1, 2, 10], the phase of the reference beam is stepped from 0 to  $2\pi$ , and a sine curve fitted to the measured intensity values to infer the phase of the object beam. For example, if the reference beam  $R$  is stepped through four values  $0, \pi/2, \pi, 3\pi/2$ ; and the corresponding intensities  $I^0, I^{\pi/2}, I^\pi$  and  $I^{3\pi/2}$  are measured, then the complex-valued object beam  $O$  can be calculated from

$$O = \frac{I^0 - I^\pi}{4} + \frac{I^{3\pi/2} - I^{\pi/2}}{4}i. \quad (2)$$

A limitation of this technique is that multiple camera acquisitions are required to obtain the phase variation across the object beam. This requires the phase drift of the system to be small over multiple camera exposures.

### 2.2. Off-Axis Holography

In off-axis holography [9, 21, 22], a slight angle is introduced between the object beam and reference beams. We consider the following mathematical expression for the intensity recorded by the camera  $I$ , which can be expanded out:

$$I = |O + R|^2 = |O|^2 + |R|^2 + OR^* + RO^*. \quad (3)$$

In the Fourier plane, the DC components  $|O|^2$  and  $|R|^2$  remain at the origin, but the tilted reference beam causes the first-order components  $OR^*$  and  $RO^*$  to be spatially offset from the origin. Taking a Fourier transform of the interferogram, cropping out the desired first-order component  $OR^*$ , translating this to the center, and taking the inverse Fourier transform allows the object beam to be recovered (Fig. 1). This approach relies on the reference beam having a uniform magnitude and flat phase profile, obtained by expanding the Gaussian beam emitted by a single-mode fiber. While computationally more demanding, this technique requires only a single camera acquisition, making it less sensitive to fast phase drift.

In the case of transmission through a multimode fiber (MMF) discussed here, the fiber's limited numerical aperture restricts the spatial frequency content of the light transmitted through the MMF. A smaller Fourier space domain can hence be used, and a more concise representation

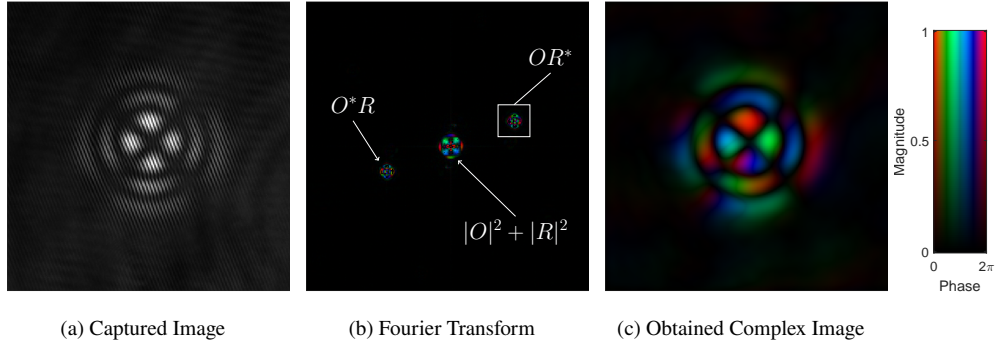


Fig. 1. Processing steps for off-axis holography. The captured image (a) is Fourier-transformed (b). The feature of interest, indicated by the  $OR^*$  square, is extracted and moved to the center of the field before an inverse Fourier transform is taken, giving the final complex field (c). The image used is that of an  $LP_{2,3}$  mode, but aberrations have not been compensated for. Larger amplitudes in Fig (b) have been clipped so that features such as the +1 and -1 orders can be seen.

obtained. This provides an alternative to downsampling [11] without leading to information loss, and gives transmission matrices of a more manageable size.

### 2.3. Common Path Reference

Phase stability between the object and reference beam can usually be achieved by ensuring that the reference beam and the object beam follow a common path, such that both are affected in the same manner by any physical effects [23–26]. However, when transmitted through a scattering system, the reference beam will form a non-uniform speckle pattern unsuitable for off-axis holography. Furthermore, it is not possible to characterize the object beam using either off-axis holography or phase stepping holography in regions where the reference beam has zero intensity.

### 2.4. Separate Path Reference

Alternatively, the reference beam can be delivered via a physically separate path [22, 27, 28]. While this makes it easier to create a reference field that is both large enough and uniform enough to characterize the entire object beam, the separate paths make it more challenging to maintain phase stability between the object beam and the reference beam. As a result, periodic reference measurements must be taken to account for any phase drift. These measurements must be taken frequently enough such that the phase drift can be reliably interpolated to any intermediary time intervals.

## 3. Experimental Setup

### 3.1. Overview of Experimental Setup

The proposed phase correction method is demonstrated using the experimental setup of Fig. 2. A collimated Gaussian beam from a single-mode fiber (SMF) is divided into a reference beam and an object beam. A second SMF delivers the reference beam to the interferometer at the output side. The object beam is modulated by a spatial light modulator (SLM) and is projected onto the input facet of the fiber under test, a 2m long,  $50\mu\text{m}$  core diameter step-index MMF with a numerical aperture of 0.22. The spatial light modulator (SLM) used is a Jasper JD8714 nematic liquid crystal on silicon device capable of 256-level phase modulation. It has a resolution of  $4\text{k} \times 2\text{k}$  with a pixel pitch of  $3.74\mu\text{m}$ . The SLM display is subdivided into an array of macro pixels for

these measurements. The sequence of lenses at the proximal side of the fiber is positioned such that the light field projected onto the fiber facet is a scaled Fourier transform of the light field in the SLM plane. This configuration allows the SLM to be tilted such that the unmodulated zeroth order is not incident on the fiber core. A phase ramp is applied to the hologram such that the modulated first order is directed to the fiber core. It is helpful to picture the modulation range of a single macro pixel as a circle on an Argand diagram in addition to the origin point.

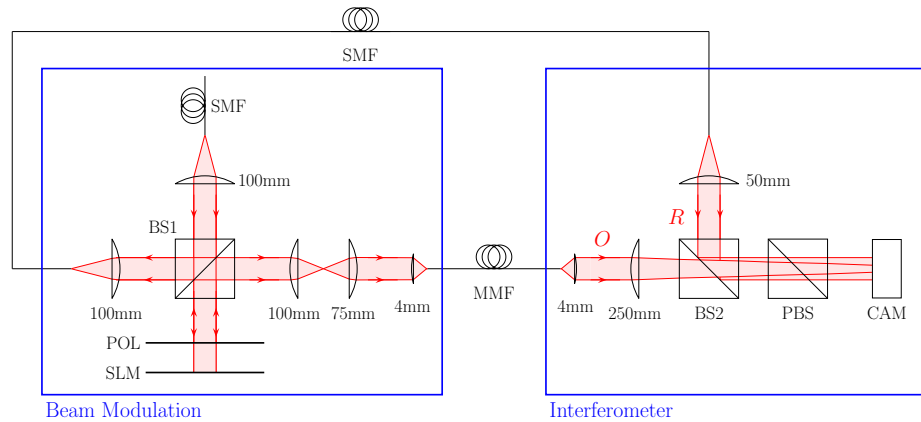


Fig. 2. Schematic of experimental setup. BS = Beam splitter; PBS = Polarizing beam splitter; SLM = Spatial light modulator; SMF = Single mode fiber; MMF = Multimode fiber; CAM = Camera; POL = Polarizer; *O* = Object Beam; *R* = Reference beam.

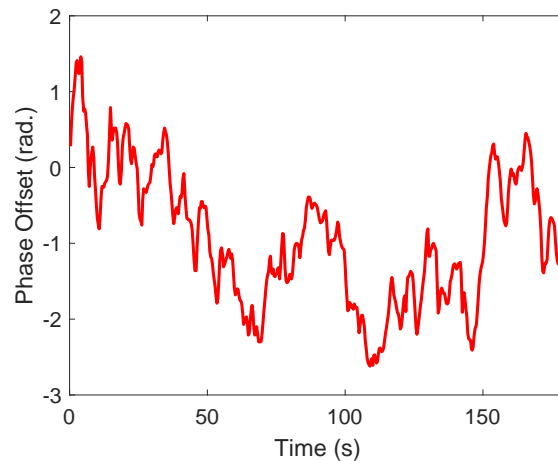


Fig. 3. The phase drift between the two arms of the interferometer is observed to be quickly varying and erratic.

The components at the distal side of the MMF form an interferometer. The field exiting the multimode fiber is magnified and imaged onto a camera to form the object beam. The reference beam exits the SMF and is collimated and mixed with the object beam in BS2. Both beams pass through a PBS to ensure a single polarization is incident on the camera. The reference beam is tilted at a slight angle relative to the object beam such that fringes are formed on the camera.

The Jasper JD8714 SLM uses pulse-width modulation to achieve 256-level phase modulation,

leading to some flicker of the projected image. This is resolved by triggering the camera off the SLM clock signal, ensuring that each image is acquired at the same point in the SLM clock cycle.

### 3.2. Phase Stability of Experimental Setup

The phase stability of the experimental system is evaluated by displaying a single hologram on the SLM and repeatedly measuring the phase observed at the interferometer. The measurement results are shown in Fig. 3, where it is seen that the phase drift is erratic, varying by up to 1 radian per second. The reasons for these fluctuations are that the experimental system was not covered, leading to airflow over the system, unisolated floor vibrations, and the fact that the object and reference arms were not of precisely equal length.

Such rapid phase drift velocities are very difficult to track by periodic phase-stepping reference measurements, as they would require a very high sampling frequency for a linear or quadratic spline interpolation of reference measurements to give a suitable approximation to intermediary time instants.

## 4. Phase Drift Correction Method

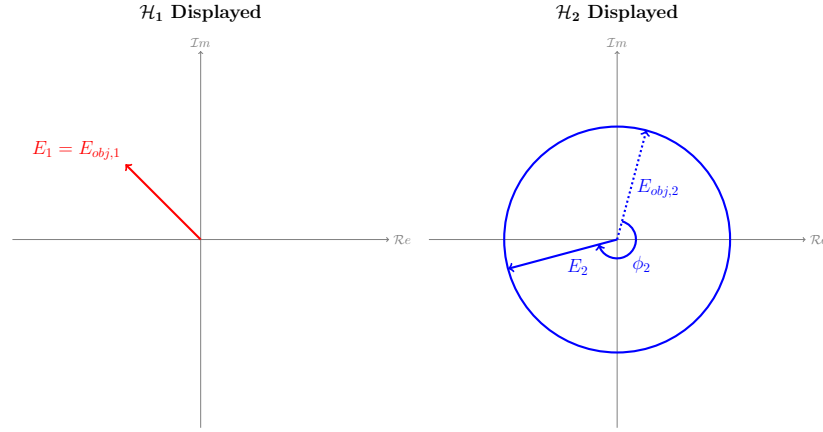
Here we demonstrate a new approach for phase-drift correction in off-axis holography. This technique is used to acquire the complex-valued fields at the output of an optical waveguide, and build the transmission matrix that describes this scattering system. To achieve this, we combine elements of a common path and a separate path reference setup. The benefits of both approaches are combined in that the reference beam is spatially uniform, while the phase stability of the measurement is preserved. As a result, off-axis interferometry becomes possible without the requirement of a slowly varying phase drift.

First, a hologram  $\mathcal{H}_1$  is displayed on the SLM and a light field  $E_1 = E_{obj,1} e^{i\phi_1}$  is observed at the fiber output, where  $e^{i\phi_1}$  describes an unknown phase drift (Fig. 4a). A second hologram  $\mathcal{H}_2$  is then displayed, and a different light field  $E_2 = E_{obj,2} e^{i\phi_2}$  is observed, where  $e^{i\phi_2}$  describes the phase drift at the instant where the second light field was recorded (Fig. 4b).  $e^{i\phi_1}$  may or may not be different to  $e^{i\phi_2}$ , as the phase stability of the system may have drifted over time. The zero-phase datum is arbitrary, and so  $\phi_1$  may be set to zero, but it is not possible to eliminate both phase drift terms in this manner. The challenge is to find a way of also eliminating the unknown phase drift term  $e^{i\phi_2}$  applied to the second measurement such that  $E_{obj,1}$  and  $E_{obj,2}$  can both be known.

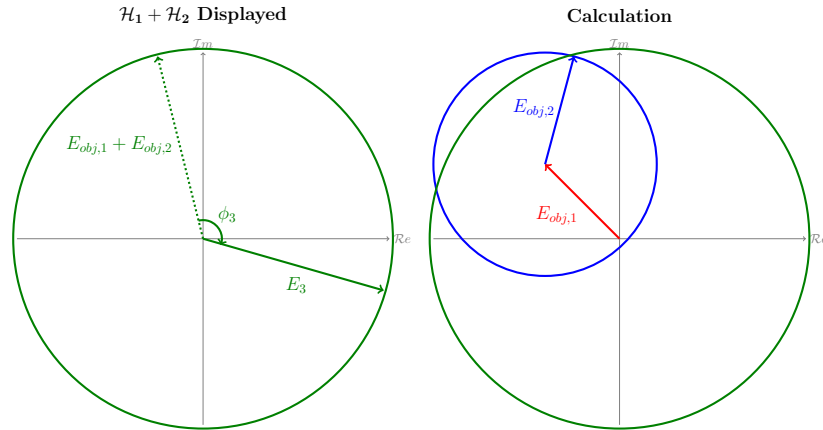
It is proposed that an additional measurement be taken. A hologram  $\mathcal{H}_1 + \mathcal{H}_2$  is displayed on the SLM, and a light field  $E_3 = (E_{obj,1} + E_{obj,2}) e^{i\phi_3}$  is observed at the fiber output. An overall unknown phase drift  $e^{i\phi_3}$  has again been incorporated, but the relative phase between  $E_{obj,1}$  and  $E_{obj,2}$  is zero (Fig. 4c).

The recorded light fields  $E_1$  and  $E_2$  can be computationally superimposed with a phase correction  $e^{i\phi_{corr}}$  applied to  $E_2$ , such that  $E_{calc} = E_1 + E_2 e^{i\phi_{corr}} = E_{obj,1} + E_{obj,2} e^{i\phi_2} e^{i\phi_{corr}}$  is calculated. When the phase correction term  $e^{i\phi_{corr}}$  corrects for the phase drift  $e^{i\phi_2}$  then  $e^{i\phi_2} e^{i\phi_{corr}} = 1$  and we denote this specific phase correction term  $e^{i\phi_{corr}^*}$ . In this case the computational superposition should match the measured field  $E_3$  to within a global phase shift  $e^{i\phi_3}$ . Applying this phase correction  $e^{i\phi_{corr}^*}$  to  $E_2$  allows  $E_{obj,2}$  to be obtained (Fig. 4d).

Fig. 4 illustrates the phase correction process for a single pixel measurement, in which case it seems possible to solve for  $\phi_{corr}^*$  using a geometric approach, but an ambiguity exists as two solutions are possible. A geometric approach is no longer available if an output image with more than one pixel is considered, but the observed ambiguity is lifted. Instead, the overlap integral can be used as a metric to determine what phase correction  $\phi_{corr}$  is appropriate:



(a)  $E_1$  is captured when  $\mathcal{H}_1$  is displayed on the SLM. This measurement defines the phase datum and consequently the phase of  $E_1$  can be considered known.  
 (b)  $E_2$  is captured when  $\mathcal{H}_2$  is displayed on the SLM. An unknown phase drift  $e^{i\phi_2}$  has occurred, and so the desired  $E_{obj,2}$  (blue dotted line) is a rotation of  $E_2$ , but it is not known which rotation (blue circle).



(c)  $E_3$  is captured when  $\mathcal{H}_1 + \mathcal{H}_2$  is displayed on the SLM. An unknown phase drift  $e^{i\phi_3}$  has occurred, and so  $E_{obj,1} + E_{obj,2}$  (dotted line) is a rotation of  $E_3$ , but it is not known which rotation (green circle).  
 (d)  $E_1$  and  $E_2$  can be computationally superimposed with different phase corrections applied to  $E_2$  (blue circle). The phase correction that correctly yields  $E_{obj,2}$  gives a superposition that coincides with a rotation of  $E_3$  (green circle).

Fig. 4. Proposed phase correction method applied to measurements with unknown phase drift. (a), (b) and (c) show the three captured measurements. (d) shows that an appropriate superposition of  $E_1$  and a phase drift-corrected  $E_2$  agrees with the measurement of  $E_3$  to within a global phase rotation around the origin.

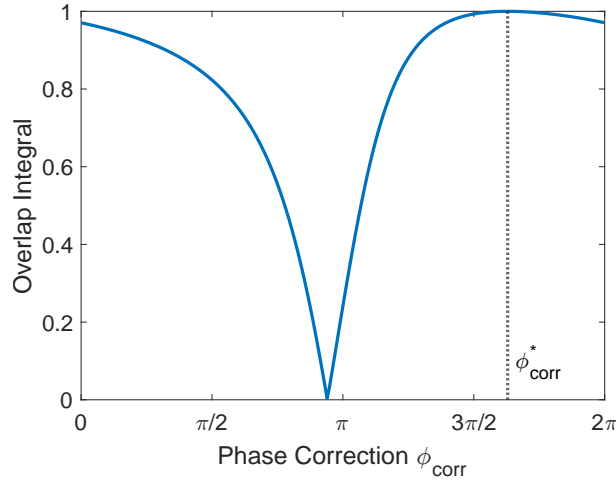


Fig. 5. Varying the phase drift correction and observing the overlap integral allows the correct phase drift correction  $\phi_{corr}^*$  to be found (dotted line).

$$\frac{\left| \int_{-\infty}^{\infty} (E_1 + E_2 e^{i\phi_{corr}}) E_3^* \right|^2}{\int_{-\infty}^{\infty} |E_1 + E_2|^2 \int_{-\infty}^{\infty} |E_3|^2}. \quad (4)$$

This metric has been chosen as it is agnostic to the global phase shift  $e^{i\phi_3}$ , giving a simpler situation where only a single parameter is to be optimized. The overlap integral metric will take on a value of 1 when  $\phi_{corr} = \phi_{corr}^*$  and it perfectly corrects for the phase drift between measurement measurements  $E_1$  and  $E_2$ .  $\phi_{corr}^*$  can then be applied to  $E_2$  to obtain two ‘in-phase’ measurements. Eq. 4 is non-linear, but is well-behaved in that it does not have any discontinuities, local minima or local maxima (Fig. 5). As such, a Golden Section search [29] has been used to maximize this function, although other more elaborate approaches could be implemented.

It has been shown here that the single additional measurement of the superimposed holograms allows the relative phase offset between the two individual holograms to be characterized. Notably, both  $E_1$  and  $E_2$  are now known, and can be used as part of the transmission matrix calculation. A sequence of  $n$  phase-corrected measurements is built up using a hologram  $\mathcal{H}_{2,n}$  that changes at each iteration and a hologram  $\mathcal{H}_1$  that is kept the same for each iteration. In this manner, each phase-corrected output  $E_{2,n}$  has a correct phase relative to  $E_1$  and hence a correct phase relative to each other phase-corrected output  $E_{2,n}$ .

The output  $E_1$  only needs to be measured a single time. Each phase-corrected  $E_2$  is then characterized using two measurements - one with  $\mathcal{H}_1$  on and one with  $\mathcal{H}_1$  off. As such,  $n$  phase-corrected input-output relationships can be characterized using  $2n$  measurements, or  $2n - 1$  measurements if  $E_1$  forms one of the input-output relationships used to calculate the transmission matrix. By comparison, standard off-axis holography would require only  $n$  measurements, whereas phase-stepping requires  $4n$  measurements.

It is unnecessary to refresh the output  $E_1$  corresponding to the hologram  $\mathcal{H}_1$ . Any change in  $E_1$  likely indicates that the measurement system or scattering medium has been perturbed and that the measurements taken are no longer valid. Here, every twentieth measurement recharacterized  $E_1$ , and overlap integrals with the first  $E_1$  measurement of more than 0.98 are consistently obtained, indicating that the system is not being altered other than by phase drift.

For the presented approach to work, it must be possible to display  $\mathcal{H}_1$  and  $\mathcal{H}_2$  as well as the superposition of  $\mathcal{H}_1 + \mathcal{H}_2$  on the phase-only SLM. This can be achieved by spatially separating

$\mathcal{H}_1$  and  $\mathcal{H}_2$  on the SLM. In this case, the inner region of the SLM is used for  $\mathcal{H}_2$ , the and outer region is used for  $\mathcal{H}_1$  (top row of in Fig. 6). In some cases an alternative approach can be used. For example, if a Hadamard basis were to be used where pixel values are allocated based on the rows of a Hadamard matrix, the hologram pixel values only take on values of +1 or -1. Pixels of the superimposed  $\mathcal{H}_1 + \mathcal{H}_2$  hologram can then only take on values of +2, 0 and -2. Rescaling these, pixel values of +1, 0 and -1 are obtained, which can be displayed on the SLM (bottom row of Fig. 6). Hence, using a Hadamard basis would allow this phase correction approach to be used without sacrificing large parts of the SLM to display a second hologram. Practically, this means that larger holograms can be used, allowing higher spatial frequencies to be projected onto the fiber facet. Other bases that superimpose  $\mathcal{H}_1$  and  $\mathcal{H}_2$  without forfeiting space on the SLM could also be envisaged, for example the matrix of randomly allocated +1, 0 and -1 pixels used by Matthès et al. [30] could equally be used.

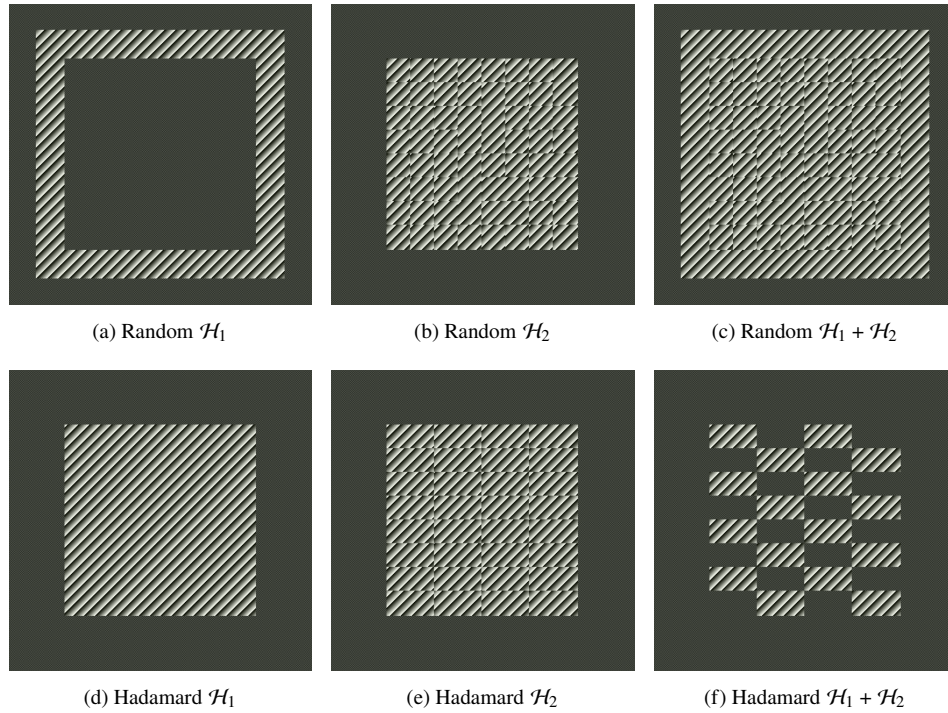


Fig. 6. A selection of holograms displayed on the SLM

## 5. Results

A  $800 \times 800$  region of the SLM is subdivided into  $20 \times 20$  macropixels to constitute the input plane. A region of  $448 \times 448$  camera pixels is acquired and downsampled in the Fourier domain to yield an output plane of  $60 \times 60$  values. A sequence of 1000 random patterns has been used to characterize a  $400 \times 3600$  transmission matrix describing propagation between the SLM input plane and the distal fiber facet output plane. Random input patterns form  $\mathcal{H}_2$  and change at each iteration.  $\mathcal{H}_1$  is formed by the outer  $1250 \times 1250$  region of the SLM, effectively forming a boundary around  $\mathcal{H}_2$  as illustrated in the top row of Fig. 6.

The acquired transmission matrix is used to reconstruct images displayed on the SLM from the complex-valued speckle patterns recorded at the distal end of the fiber (Fig. 7). Poor agreement is observed between the displayed images and the reconstructed images when no phase

correction is employed, as the measurement has been perturbed by the substantial phase drift of the experimental system (Fig. 3). Excellent agreement is observed when the proposed phase correction algorithm is used, indicating that this approach corrects for any experimental phase drift and that the transmission matrix is correctly acquired. Imaging error has been quantified using a phase-error metric  $\text{Err}_{\text{phase}}$ , comparing the displayed pattern  $E_{\text{displayed}}$  with the estimated pattern  $E_{\text{estimated}}$ ,

$$\text{Err}_{\text{phase}} = \frac{\sum |\angle E_{\text{estimated}} - \angle E_{\text{displayed}}|}{N}. \quad (5)$$

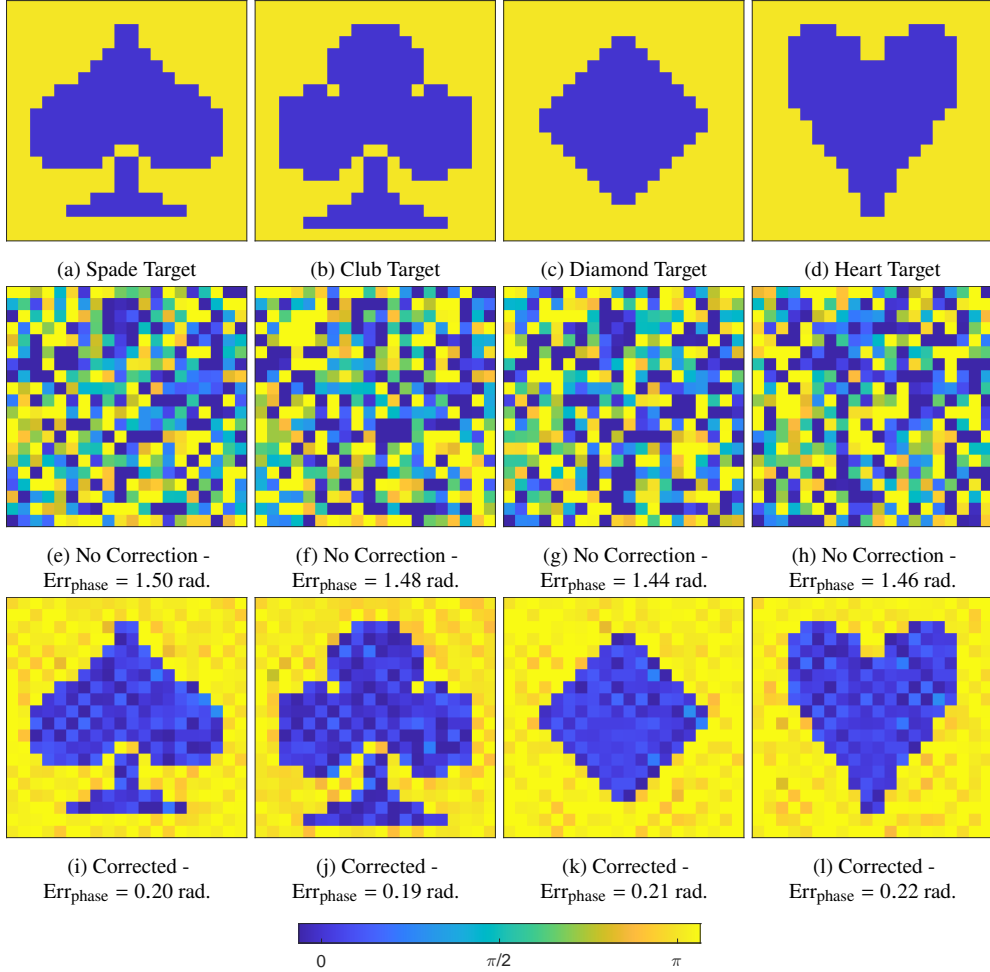


Fig. 7. The top row shows the phase pattern displayed on the SLM. Without phase drift correction the transmission matrix is incorrectly acquired and the images cannot be faithfully reconstructed (middle row). The proposed phase drift correction algorithm allows the transmission matrix to be correctly acquired, and the images to be reconstructed (bottom row).

## 6. Conclusions

We have presented a method for phase correction in off-axis holography experiments. The proposed technique works even if the phase drift is exceptionally fast, as long as the phase

does not drift significantly within a single camera exposure. Our method allows the stability requirements of the interferometer setups to be relaxed and more challenging measurements to be performed. While we have demonstrated proof of principle using a multimode fibre, other scattering media such as titania or biological tissue could equally be considered. This approach is hence more widely applicable, and will be pertinent to the development of hair-thin endoscopes and microscopes capable of imaging deep into scattering tissue.

## Funding

The authors wish to thank the Engineering and Physical Sciences Research Council (EP/L015889/1, EP/T008369/1, EP/V055003/1 and EP/L016567/1) for financial support during the period of this research. GSDG acknowledges support from a UKRI Future Leaders Fellowship (MR/T041951/1). TGE acknowledges support from the Leverhulme Trust (Research Project Grant RPG-2018-256) during the period of this research. The authors would like to thank Optalysys for supplying the SLM used in these experiments.

## Disclosures

The authors declare no conflicts of interest.

## Data Availability

Data underlying the results presented in this paper are not publicly available at this time but may be obtained from the authors upon reasonable request.

## References

1. I. M. Vellekoop and A. P. Mosk, "Focusing coherent light through opaque strongly scattering media," *Opt. Lett.* **32**, 2309 (2007).
2. S. M. Popoff, G. Lerosey, R. Carminati, M. Fink, A. C. Boccara, and S. Gigan, "Measuring the transmission matrix in optics: An approach to the study and control of light propagation in disordered media," *Phys. Rev. Lett.* **104** (2010).
3. S. Popoff, G. Lerosey, M. Fink, A. C. Boccara, and S. Gigan, "Image transmission through an opaque material," *Nat. Commun.* **1** (2010).
4. I. M. Vellekoop, A. Lagendijk, and A. P. Mosk, "Exploiting disorder for perfect focusing," *Nat. Photonics* **4**, 320–322 (2010).
5. Z. Yaqoob, D. Psaltis, M. S. Feld, and C. Yang, "Optical phase conjugation for turbidity suppression in biological samples," *Nat. Photonics* **2**, 110–115 (2008).
6. X. Yang, Y. Pu, and D. Psaltis, "Imaging blood cells through scattering biological tissue using speckle scanning microscopy," *Opt. Express* **22**, 3405 (2014).
7. H. Yu, J. Park, K. Lee, J. Yoon, K. Kim, S. Lee, and Y. Park, "Recent advances in wavefront shaping techniques for biomedical applications," *Curr. Appl. Phys.* **15**, 632 – 641 (2015).
8. T. Čižmár and K. Dholakia, "Exploiting multimode waveguides for pure fibre-based imaging," *Nat. Commun.* **3**, 1027 (2012).
9. Y. Choi, C. Yoon, M. Kim, T. D. Yang, C. Fang-Yen, R. R. Dasari, K. J. Lee, and W. Choi, "Scanner-free and wide-field endoscopic imaging by using a single multimode optical fiber," *Phys. Rev. Lett.* **109** (2012).
10. A. M. Caravaca-Aguirre and R. Piestun, "Single multimode fiber endoscope," *Opt. Express* **25**, 1656–1665 (2017).
11. G. S. D. Gordon, R. Mouthaan, T. D. Wilkinson, and S. E. Bohndiek, "Coherent imaging through multicore fibres with applications in endoscopy," *J. Light. Technol.* **37**, 5733–5745 (2019).
12. G. S. D. Gordon, J. Joseph, M. P. Alcolea, T. Sawyer, C. Williams, C. R. M. Fitzpatrick, P. H. Jones, M. di Pietro, R. C. Fitzgerald, T. D. Wilkinson, and S. E. Bohndiek, "Quantitative phase and polarization imaging through an optical fiber applied to detection of early esophageal tumorigenesis," *J. Biomed. Opt.* **24**, 1 – 13 (2019).
13. V. Durán, F. Soldevila, E. Irls, P. Clemente, E. Tajahuerce, P. Andrés, and J. Lancis, "Compressive imaging in scattering media," *Opt. Express* **23**, 14424 (2015).
14. S. M. Popoff, G. Lerosey, M. Fink, A. C. Boccara, and S. Gigan, "Controlling light through optical disordered media: transmission matrix approach," *New J. Phys.* **13**, 123021 (2011).
15. S. Rotter and S. Gigan, "Light fields in complex media: Mesoscopic scattering meets wave control," *Rev. Mod. Phys.* **89**, 015005 (2017).
16. A. Ymeti, J. Greve, P. V. Lambeck, R. Wijn, R. G. Heideman, and J. S. Kanger, "Drift correction in a multichannel integrated optical young interferometer," *Appl. optics* **44**, 3409–3412 (2005).

17. A. Azari, E. Mohajerani, Z. Abedi, and A. Shams, "Interferometry technique to eliminate noise in interference data based on a mach–zehnder interferometer," *Appl. optics* **53**, 1734–1738 (2014).
18. A. A. Freschi and J. Frejlich, "Adjustable phase control in stabilized interferometry," *Opt. Lett.* **20**, 635–637 (1995).
19. P. Roztockı, B. MacLellan, M. Islam, C. Reimer, B. Fischer, S. Sciara, R. Helsten, Y. Jestin, A. Cino, S. T. Chu *et al.*, "Arbitrary phase access for stable fiber interferometers," *Laser & Photonics Rev.* p. 2000524 (2021).
20. B. P. Abbott, R. Abbott, T. Abbott, M. Abernathy, F. Acernese, K. Ackley, C. Adams, T. Adams, P. Addesso, R. Adhikari *et al.*, "Observation of gravitational waves from a binary black hole merger," *Phys. review letters* **116**, 061102 (2016).
21. N. Verrier and M. Atlan, "Off-axis digital hologram reconstruction: Some practical considerations," *Appl. Opt.* **50** (2011).
22. D. Loterie, S. Farahi, I. Papadopoulos, A. Goy, D. Psaltis, and C. Moser, "Digital confocal microscopy through a multimode fiber," *Opt. Express* **23**, 23845 (2015).
23. S. Sivankutty, E. R. Andresen, R. Cossart, G. Bouwmans, S. Monneret, and H. Rigneault, "Ultra-thin rigid endoscope: two-photon imaging through a graded-index multi-mode fiber," *Opt. Express* **24**, 825 (2016).
24. S. Bianchi and R. Di Leonardo, "A multi-mode fiber probe for holographic micromanipulation and microscopy," *Lab Chip* **12**, 635–639 (2012).
25. H. Zhang, B. Zhang, and Q. Liu, "Oam-basis transmission matrix in optics: a novel approach to manipulate light propagation through scattering media," *Opt. Express* **28**, 15006 (2020).
26. L. Collard, F. Pisano, M. Pisanello, A. Balena, M. De Vittorio, and F. Pisanello, "Wavefront engineering for controlled structuring of far-field intensity and phase patterns from multimodal optical fibers," *APL Photonics* **6**, 051301 (2021).
27. T. Čižmár and K. Dholakia, "Shaping the light transmission through a multimode optical fibre: complex transformation analysis and applications in biophotonics," *Opt. Express* **19**, 18871 (2011).
28. M. Plöschner, B. Straka, K. Dholakia, and T. Čižmár, "Gpu accelerated toolbox for real-time beam-shaping in multimode fibres," *Opt. Express* **22**, 2933 (2014).
29. W. H. Press, S. A. Teukolsky, W. T. Vetterling, and B. P. Fannery, *Numerical Recipes* (Cambridge University Press, 2007), 3rd ed.
30. M. W. Matthès, Y. Bromberg, J. de Rosny, and S. M. Popoff, "Learning and avoiding disorder in multimode fibers," *Phys. Rev. X* **11**, 021060 (2021).